RESEARCH ARTICLE

Ultrasensitive Detection of Circulating LINE-1 ORF1p as a Specific Multicancer Biomarker

Martin S. Taylor[1], Connie Wu[1,2], Peter C. Fridy[3], Stephanie J. Zhang[1,2], Yasmeen Senussi[1,2], Justina C. Wolters[4], Tatiana Cajuso[5], Wen-Chih Cheng[5], John D. Heaps[5], Bryant D. Miller[5], Kei Mori[1,6], Limor Cohen[1,2,7], Hua Jiang[3], Kelly R. Molloy[8], Brian T. Chait[8], Michael G. Goggins[9], Irun Bhan[10], Joseph W. Franses[10], Xiaoyu Yang[11], Mary-Ellen Taplin[11], Xinan Wang[12], David C. Christiani[10,12], Bruce E. Johnson[11], Matthew Meyerson[11], Ravindra Uppaluri[13], Ann Marie Egloff[13], Elyssa N. Denault[10], Laura M. Spring[10], Tian-Li Wang[9], Ie-Ming Shih[9], Jennifer E. Fairman[9], Euihye Jung[14], Kshitij S. Arora[1], Osman H. Yilmaz[15], Sonia Cohen[16], Tatyana Sharova[16], Gary Chi[10], Bryanna L. Norden[10], Yuhui Song[10], Linda T. Nieman[10], Leontios Pappas[10], Aparna R. Parikh[10], Matthew R. Strickland[10], Ryan B. Corcoran[10], Tomas Mustelin[17], George Eng[1,18], Ömer H. Yilmaz[1,18], Ursula A. Matulonis[11], Andrew T. Chan[22], Steven J. Skates[19], Bo R. Rueda[20], Ronny Drapkin[14], Samuel J. Klempner[10], Vikram Deshpande[1], David T. Ting[10], Michael P. Rout[3], John LaCava[3,21], David R. Walt[1,2], and Kathleen H. Burns[1,5]

ABSTRACT

Improved biomarkers are needed for early cancer detection, risk stratification, treatment selection, and monitoring treatment response. Although proteins can be useful blood-based biomarkers, many have limited sensitivity or specificity for these applications. Long INterspersed Element-1 (LINE-1) open reading frame 1 protein (ORF1p) is a transposable element protein overexpressed in carcinomas and high-risk precursors during carcinogenesis with negligible expression in normal tissues, suggesting ORF1p could be a highly specific cancer biomarker. To explore ORF1p as a blood-based biomarker, we engineered ultrasensitive digital immunoassays that detect mid-attomolar (10^{-17} mol/L) ORF1p concentrations in plasma across multiple cancers with high specificity. Plasma ORF1p shows promise for early detection of ovarian cancer, improves diagnostic performance in a multianalyte panel, provides early therapeutic response monitoring in gastroesophageal cancers, and is prognostic for overall survival in gastroesophageal and colorectal cancers. Together, these observations nominate ORF1p as a multicancer biomarker with potential utility for disease detection and monitoring.

SIGNIFICANCE: The LINE-1 ORF1p transposon protein is pervasively expressed in many cancers and is a highly specific biomarker of multiple common, lethal carcinomas and their high-risk precursors in tissue and blood. Ultrasensitive ORF1p assays from as little as 25 μL plasma are novel, rapid, cost-effective tools in cancer detection and monitoring.

See related commentary by Doucet and Cristofari, p. 2502.

[1]Department of Pathology, Mass General Brigham and Harvard Medical School, Boston, Massachusetts. [2]Wyss Institute for Biologically Inspired Engineering at Harvard University, Boston, Massachusetts. [3]Laboratory of Cellular and Structural Biology, The Rockefeller University, New York, New York. [4]Department of Pediatrics, University of Groningen, University Medical Center Groningen, Groningen, the Netherlands. [5]Department of Pathology, Dana-Farber Cancer Institute and Harvard Medical School, Boston, Massachusetts. [6]Healthcare Optics Research Laboratory, Canon U.S.A., Inc., Cambridge, Massachusetts. [7]Department of Chemistry and Chemical Biology, Harvard University, Cambridge, Massachusetts. [8]Laboratory of Mass Spectrometry and Gaseous Ion Chemistry, The Rockefeller University, New York, New York. [9]Johns Hopkins University School of Medicine, Baltimore, Maryland. [10]Mass General Cancer Center and Department of Medicine, Massachusetts General Hospital and Harvard Medical School, Boston, Massachusetts. [11]Department of Medical Oncology, Dana-Farber Cancer Institute and Harvard Medical School, Boston, Massachusetts. [12]Department of Environmental Health, Harvard T.H. Chan School of Public Health, Harvard University, Boston, Massachusetts. [13]Department of Surgery, Brigham and Women's Hospital and Harvard Medical School, Boston, Massachusetts. [14]University of Pennsylvania Perelman School of Medicine, Philadelphia, Pennsylvania. [15]Department of Pathology, Beth Israel Deaconess Medical Center and Harvard Medical School, Boston, Massachusetts. [16]Department of Surgery, Massachusetts General Hospital and Harvard Medical School, Boston, Massachusetts. [17]Division of Rheumatology, Department of Medicine, University of Washington, Seattle, Washington. [18]The David H. Koch Institute for Integrative Cancer Research

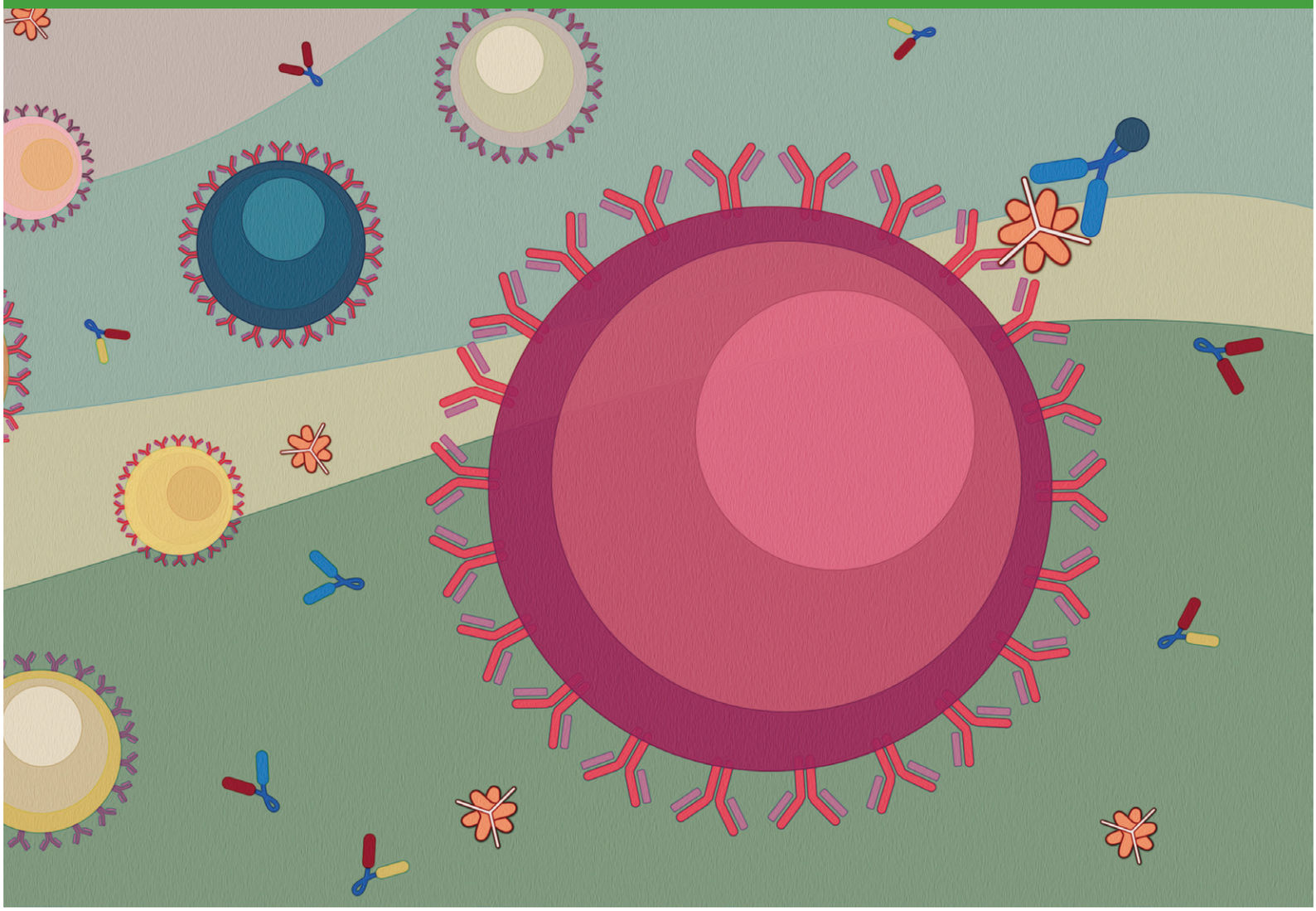

INTRODUCTION

There is a significant clinical need for noninvasive methods to detect, risk stratify, and monitor cancers over time. Many malignancies are diagnosed at late stages when the disease is widespread, contributing significantly to cancer morbidity and mortality (1). In contrast, there is a likely window in early-stage disease when patients are typically asymptomatic, in which treatments can be much more effective. Biomarkers are also needed to assess the likelihood of progression in patients with precursor lesions, to provide prognostic information, and to predict and monitor responses or resistance to treatment (2). Considerable advances have been made toward detecting circulating tumor

at MIT, Department of Biology, Massachusetts Institute of Technology, Cambridge, Massachusetts. [19]MGH Biostatistics, Massachusetts General Hospital and Harvard Medical School, Boston, Massachusetts. [20]Department of Obstetrics and Gynecology, Massachusetts General Hospital, and Harvard Medical School, Boston, Massachusetts. [21]European Research Institute for the Biology of Ageing, University Medical Center Groningen, Groningen, the Netherlands. [22]Clinical and Translational Epidemiology Unit and Division of Gastroenterology, Massachusetts General Hospital and Harvard Medical School, Boston, Massachusetts.

Note: M.S. Taylor and C. Wu contributed equally to this article.

David R. Walt and Kathleen H. Burns share senior corresponding authorship.

Current address for Connie Wu: University of Michigan Life Sciences Institute, Department of Biomedical Engineering, Ann Arbor, MI; and current address for Kshitij S. Arora, Department of Pathology, Louisiana State University Health, Shreveport, LA.

Corresponding Authors: Kathleen H. Burns, 450 Brookline Avenue, Mayer Building 641, Dana-Farber Cancer Institute, Boston, MA 02215. E-mail: kathleenh_burns@dfci.harvard.edu; Martin S. Taylor, Department of Pathology, Dana-Farber Cancer Institute, 450 Brookline Avenue, Boston, MA 02215. E-mail: mstaylor@mgh.harvard.edu; Connie Wu, 210 Washtenaw Avenue, Life Sciences Institute, University of Michigan, Ann Arbor, MI 48109. E-mail: conniewu@umich.edu; and David R. Walt, Department of Pathology, Mass General Brigham, 60 Fenwood Road, Boston, MA 02115. E-mail: dwalt@bwh.harvard.edu; E-mail: achan@mgh.harvard.edu

Cancer Discov 2023;13:2532–47

doi: 10.1158/2159-8290.CD-23-0313

DNA, circulating tumor cells, microRNAs, and extracellular vesicles as noninvasive cancer biomarkers (3). However, achieving high sensitivities and specificities, particularly in affordable, scalable, clinical-grade screening assays for early cancer detection, remains a major challenge. The plasma proteome provides a rich reservoir of potential biomarkers (4), which may be used individually or in combination for multicancer early detection (MCED) assays (5). However, most readily detectable proteins, including CA125 and HE4 (6), FDA-cleared markers for the differential diagnosis of pelvic masses, are not sufficiently sensitive at the required high specificity (7) for cancer screening and/or are expressed in normal tissues and therefore lack the requisite specificity.

We have previously shown that expression of Long INterspersed Element-1 (L1, LINE-1)–encoded open reading frame 1 protein (ORF1p) is a hallmark of many cancers (8), particularly p53-deficient epithelial cancers. These encompass many of the most commonly occurring and lethal human cancers, including esophageal, colorectal, lung, breast, prostate, ovarian, uterine, pancreatic, and head and neck cancers. L1 is the only active protein-coding transposon in humans. We each inherit, dispersed throughout our genomes, a complement of active L1 loci encoding two proteins: ORF1p, the highly expressed RNA binding protein (8), and ORF2p, an endonuclease and reverse transcriptase with limited expression (9) that generates L1 insertions in cancer genomes (10–13). L1 expression is repressed in normal somatic tissues, resulting in either very low or undetectable levels of L1 protein (9, 14). Epigenetic dysregulation of L1 and L1 ORF1p overexpression begins early in carcinogenesis, and histologic precursors of ovarian, esophageal, colorectal, and pancreatic cancers studied all express ORF1p at varying levels (8, 15). ORF1p is thus a promising cancer biomarker.

Although elevated expression of ORF1p is readily detected by immunostaining in tumor tissue, ORF1p is found in plasma at low concentrations, well below detection limits of conventional clinical laboratory methods. We, therefore, applied the much more sensitive Single-Molecule Arrays (Simoa), a digital bead-based ELISA technology, and in preliminary studies detected ORF1p in plasma at femtomolar levels in subsets of patients with advanced breast (33%, $n = 6$; ref. 16) and colorectal (90%, $n = 32$; ref. 17) cancers, respectively. Here, we assess the landscape of ORF1p plasma levels across multiple cancers, iteratively develop highly sensitive assays for potential applications in early or minimal residual disease detection, and provide evidence that plasma ORF1p may be an early indicator of therapeutic response.

RESULTS

Because our preliminary survey of plasma ORF1p levels by Simoa in patients with advanced-stage colorectal cancer indicated detectable ORF1p levels in 90% of cases (17), higher than the proportion of colorectal cancers we previously reported to express ORF1p by IHC (50%, $n = 18$; ref. 8), we first sought to benchmark ORF1p in tissues. Using a reoptimized protocol (8), we stained 211 colorectal cancers [178 sequential cases included on a tissue microarray (TMA) as well as an additional 33 with matched plasma] and found 91% of colorectal cancer cases were immunoreactive for ORF1p (Fig. 1A). This result is consistent with genetic studies demonstrating somatic L1 retrotransposition in most colorectal cancers (18), including activity in precancerous lesions antedating *APC* tumor suppressor loss (19–21). Similarly, genetic evidence shows esophageal adenocarcinoma (EAC) has high L1 activity (12), and L1 insertions occur in the highly prevalent Barrett esophagus (BE) precursor early in carcinogenesis (22, 23). We therefore assembled a cross-sectional cohort of 72 BE cases with consensus diagnosis reached by three expert gastrointestinal pathologists from two institutions. L1 RNA and ORF1p expression were pervasive in dysplastic BE and present in 100% of 51 esophageal carcinomas (Fig. 1B and C); all five BE cases indefinite for dysplasia and positive for ORF1p and/or L1 RNA developed high-grade dysplasia on subsequent biopsies. Overall, this picture is similar to high-grade serous ovarian cancers (HGSOC), where ORF1p is expressed in 90% of cases and 90% of fallopian tube precursor lesions (serous tubal intraepithelial carcinomas, STIC; refs. 8, 15, 24). The cumulative ORF1p staining data to date across carcinomas are summarized in Fig. 1D. Taken together, ORF1p tissue expression is highly prevalent in gastrointestinal and gynecologic carcinomas and high-risk precursor lesions.

We next sought to extend our tissue findings and explore plasma ORF1p. We optimized our previously reported ORF1p Simoa assay and assessed the landscape of ORF1p levels in pretreatment plasma from patients with advanced cancers. This "first-generation" assay uses a recombinant, single-domain camelid nanobody (Nb5) as the capture reagent and a monoclonal antibody (Ab6) as the detector reagent and has a limit of detection of 0.056 pg/mL (~470 aM trimeric ORF1p), corresponding to 1.9 fM in plasma after correcting for sample dilution (Fig. 2A; Supplementary Table S1). With this assay, we surveyed multiple cancer types and >400 "healthy" control individuals, who were without known cancer at the time blood was donated to the biobank. Plasma ORF1p appears to be a highly specific cancer biomarker, with undetectable levels in ~99% of controls (ages 20–90; Fig. 2B; Supplementary Fig. S1A–S1C). Of the five control patients with detectable ORF1p, the one with the highest ORF1p was found six months later to have advanced prostate cancer and 19 months later a cutaneous T-cell lymphoma; limited clinical information is available for the other four positive "healthy" individuals. With a cutoff set at 98% specificity in "healthy" controls, the highest proportions of ORF1p$^+$ cases were observed in colorectal (58%, $n = 101$) and ovarian cancers (71%, $n = 145$). Although most of these patients had advanced-stage disease, plasma ORF1p remained detectable in several early-stage patients in the cohort, including in those with ovarian and lung cancers and in 5 of 18 with intraductal papillary mucinous neoplasms in the pancreas (IPMN; Supplementary Figs. S2–S4). Notably, four of eight stage I ovarian cancers in the cohort were positive (Supplementary Fig. S2), suggesting that plasma ORF1p may be an indicator of early-stage disease. As L1 expression is also dysregulated in autoimmune disease and autoantibodies against ORF1p are prevalent in patients with systemic lupus erythematosus (SLE), we measured plasma ORF1p in 30 SLE patients and observed no detectable levels (Supplementary Fig. S5; ref. 25). Detectable ORF1p

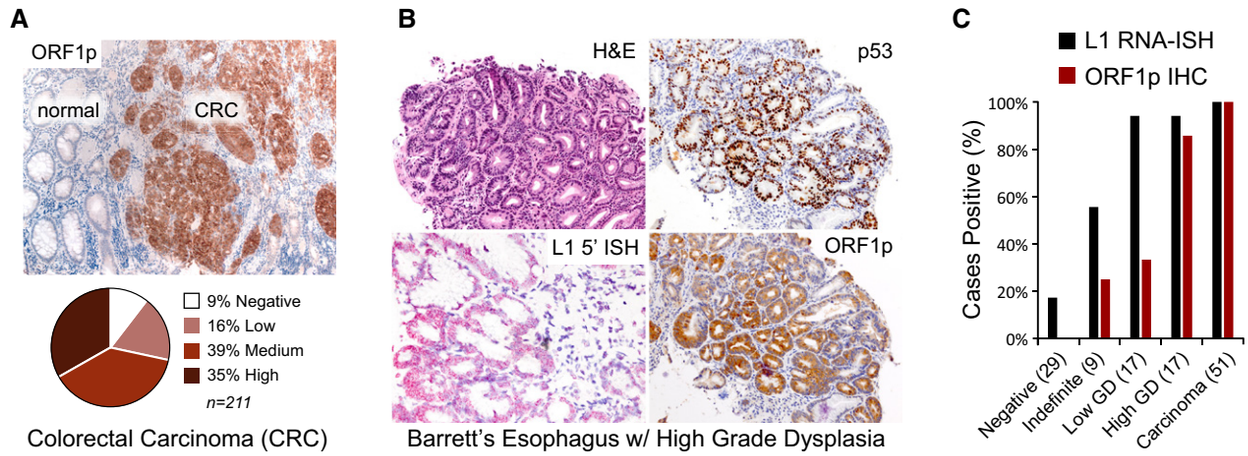

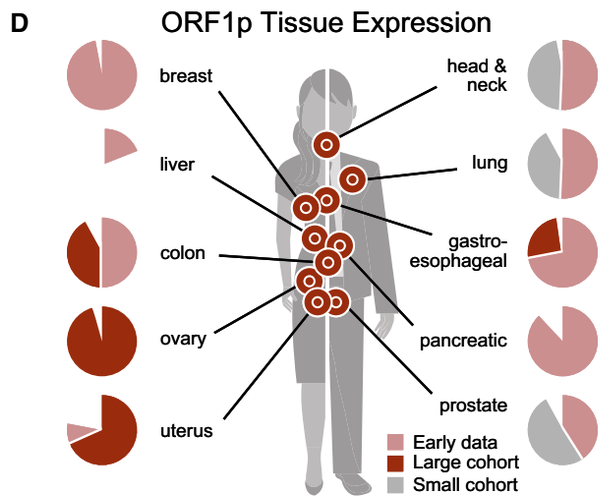

Figure 1. ORF1p expression is early and pervasive in carcinomas. **A,** ORF1p immunostaining in a cohort of 211 colorectal cancers (CRC). **B,** Representative BE case: lesional cells overexpress p53, the L1 RNA, and ORF1p. H&E, hematoxylin and eosin; ISH, *in situ* hybridization. **C,** L1 RNA and ORF1p overexpression across a cohort of 72 consensus BE cases and 51 carcinomas. GD, grade dysplasia. **D,** Summary overview of current data on ORF1p tissue expression in carcinomas (by IHC); early data are from Rodić et al. (8), large cohort colon and gastroesophageal and small cohorts ($n < 30$) are from this study, and large cohort ovarian and uterine are from Pisanic et al. (15) and Xia et al. (24). Large and small cohort ovarian data both showed >90% expression of ORF1p.

was seen in 1 of 30 patients with chronic liver disease; the one positive patient was subsequently diagnosed with hepatocellular carcinoma (Supplementary Fig. S5). Size exclusion chromatography analysis of patient plasma further showed that the majority of ORF1p resides outside extracellular vesicles (Supplementary Fig. S6A and S6B). Genomics analysis was available for a subset of patients in the lung cancer patient cohort ($n = 32$); interestingly, detectable plasma ORF1p was associated with more genomic amplifications, higher tumor mutational burden ($P = 0.02$ and 0.007, respectively, Wilcoxon test; Supplementary Fig. S7A), and tended to have more *TP53* mutations and fewer *KRAS* mutations (Supplementary Fig. S7B). ORF1p did not correlate with PSA levels in prostate cancer patients (Supplementary Fig. S8). Together, these findings support the hypothesis that tumor-derived ORF1p can be found in the peripheral blood of cancer patients and may act as a cancer-specific biomarker.

Given the gap between proportions of ORF1p$^+$ cancers by tumor IHC (~90% for colorectal cancer and HGSOC) versus by blood testing (~60%–70%), we evaluated the possibility of increasing plasma assay sensitivity by decreasing the assay's lower limit of detection. To this end, we developed a panel of ORF1p affinity reagents, including new recombinant rabbit monoclonal antibodies (RabMAb) and engineered camelid nanobodies raised against recombinant human ORF1p. Because ORF1p is homotrimeric, we engineered multimeric nanobody reagents with the goal of enhancing binding affinity via increased avidity. These parallel development efforts ultimately yielded both improved nanobody and rabbit monoclonal antibody reagents with at least low-picomolar equilibrium dissociation constants (K_D; Supplementary Figs. S9–S14; Supplementary Tables S2–S4). Monoclonal antibodies were further validated by western blotting (Supplementary Fig. S15). Iterative screening of these reagents with Simoa using recombinant antigen and select patient plasma samples yielded three best-performing capture::detection pairs, termed "second-generation," which use rabbit monoclonal antibodies 34H7 and 62H12 as capture reagents and either Ab6 or homodimeric form of Nb5 (Nb5-5LL) as detector (Fig. 3A–C; Supplementary Figs. S16–S19). Adding detergent further improved performance by limiting bead aggregation and improving bead loading into microwells. These second-generation assays achieve detection limits of 0.016 to 0.029 pg/mL (130–240 aM trimeric ORF1p), and the four different reagents have predominantly nonoverlapping epitopes in binning experiments (34H7 and 62H12 partially overlap; Fig. 3A and B; Supplementary Tables S1, S5, and S6). Somewhat unexpectedly, analytical sensitivity of the assay (for detecting

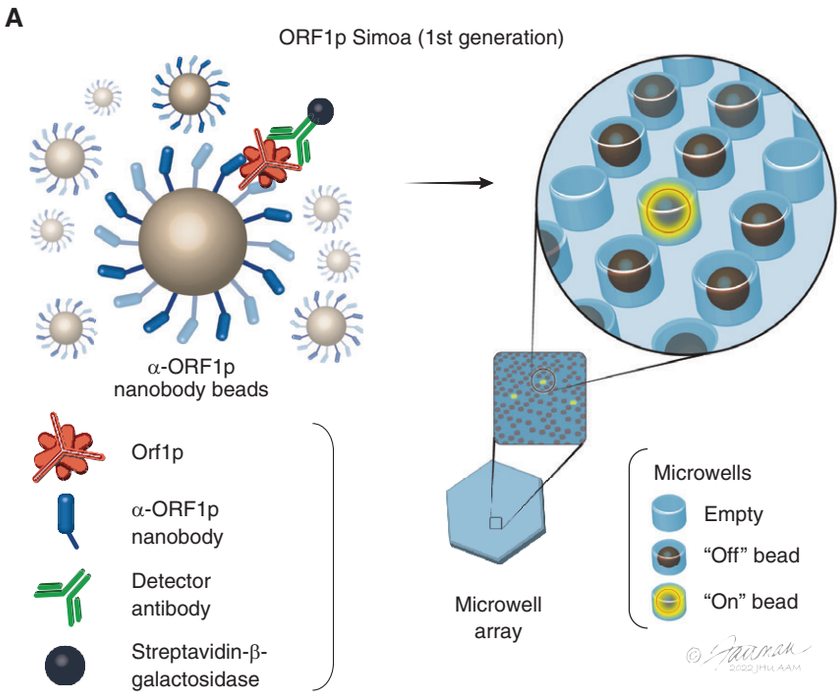

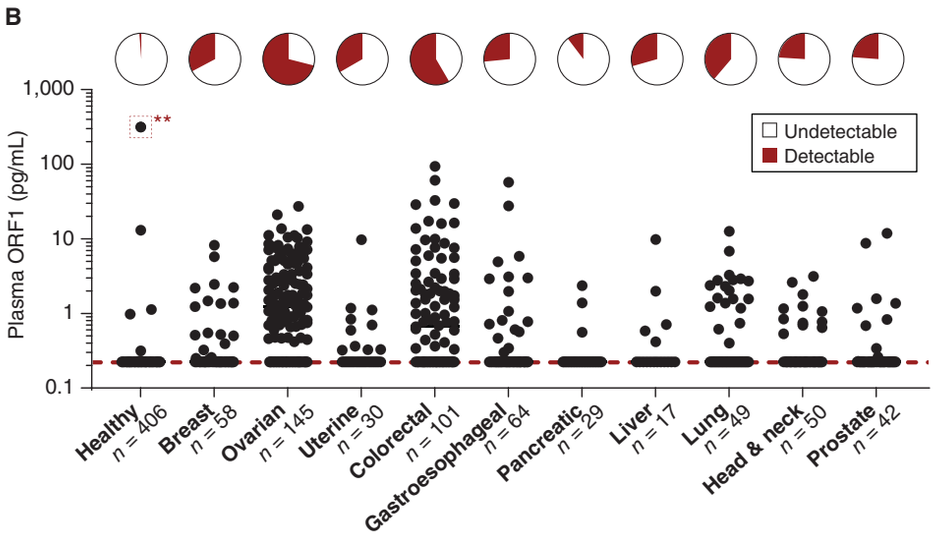

Figure 2. Highly specific detection of carcinomas with the first-generation ORF1p Simoa assay. **A,** Schematic of single-molecule protein detection by Simoa; a first-generation assay is shown. Antibody/nanobody-coated magnetic beads, present in excess relative to target, capture single target ORF1p molecules; in the first-generation assay, beads are conjugated with α-ORF1p capture nanobody 5 (Nb5). Enzyme-labeled α-ORF1p detection reagent (here, an antibody, Ab6) is added, forming an "immunosandwich," beads are loaded into microwells that each can hold at most one bead, and ORF1p molecules are then digitally detected using a fluorogenic substrate by counting "on" wells. Illustration: Jennifer E. Fairman, CMI, FAMI. © 2023 Johns Hopkins University, AAM. **B,** First-generation ORF1p Simoa detects plasma ORF1p with high specificity across major carcinomas. Pie charts indicate the percentage of samples with detectable levels; dashed red line, limit of detection. **, This patient was thought to be "healthy" at the time of blood donation but was six months later found to have prostate cancer and 19 months later found to have lymphoma. (*Illustration: Jennifer E. Fairman, CMI, FAMI, © 2023 JHU AAM Department of Art as Applied to Medicine, The Johns Hopkins University School of Medicine*).

recombinant ORF1p in buffer) did not perfectly correspond to clinical sensitivity (for detecting ORF1p in cancer patient plasma). Although the second-generation assays demonstrated less than an order-of-magnitude improvement in analytical sensitivity over the first-generation assay, they showed considerable improvement in circulating ORF1p detectability over background in buffer in remeasured samples across a large cohort of healthy and cancer patients (Fig. 3B; Supplementary Fig. S20A and S20B). This difference may be due to differing accessibilities of circulating ORF1p epitopes or to different nonspecific binding patterns in plasma.

Undetectable or extremely low ORF1p levels in healthy individuals could readily be discriminated from measured ORF1p levels in ovarian cancer patients, resulting in a strong discriminatory ability with single-marker models (area under the receiver-operating characteristic curve, AUCs of 0.93 to 0.948, sensitivity of 41% to 81% at 98% specificity; Fig. 3D top panel; Supplementary Table S7). This large cohort included pretreatment plasma samples from a subcohort of ovarian cancer patients (mostly high-grade serous ovarian carcinoma, "Penn cohort") with age-matched controls (n = 51–53 women; Fig. 3C); again, second-generation assays showed higher sensitivities while maintaining high specificities, notably achieving detection of five out of six stage I/II patients at >98% specificity. Furthermore, multivariate models combining ORF1p (34H7::Nb5-5LL assay) with ovarian cancer biomarkers CA125 and HE4 yielded improved diagnostic performance over these existing markers (CA125 and HE4

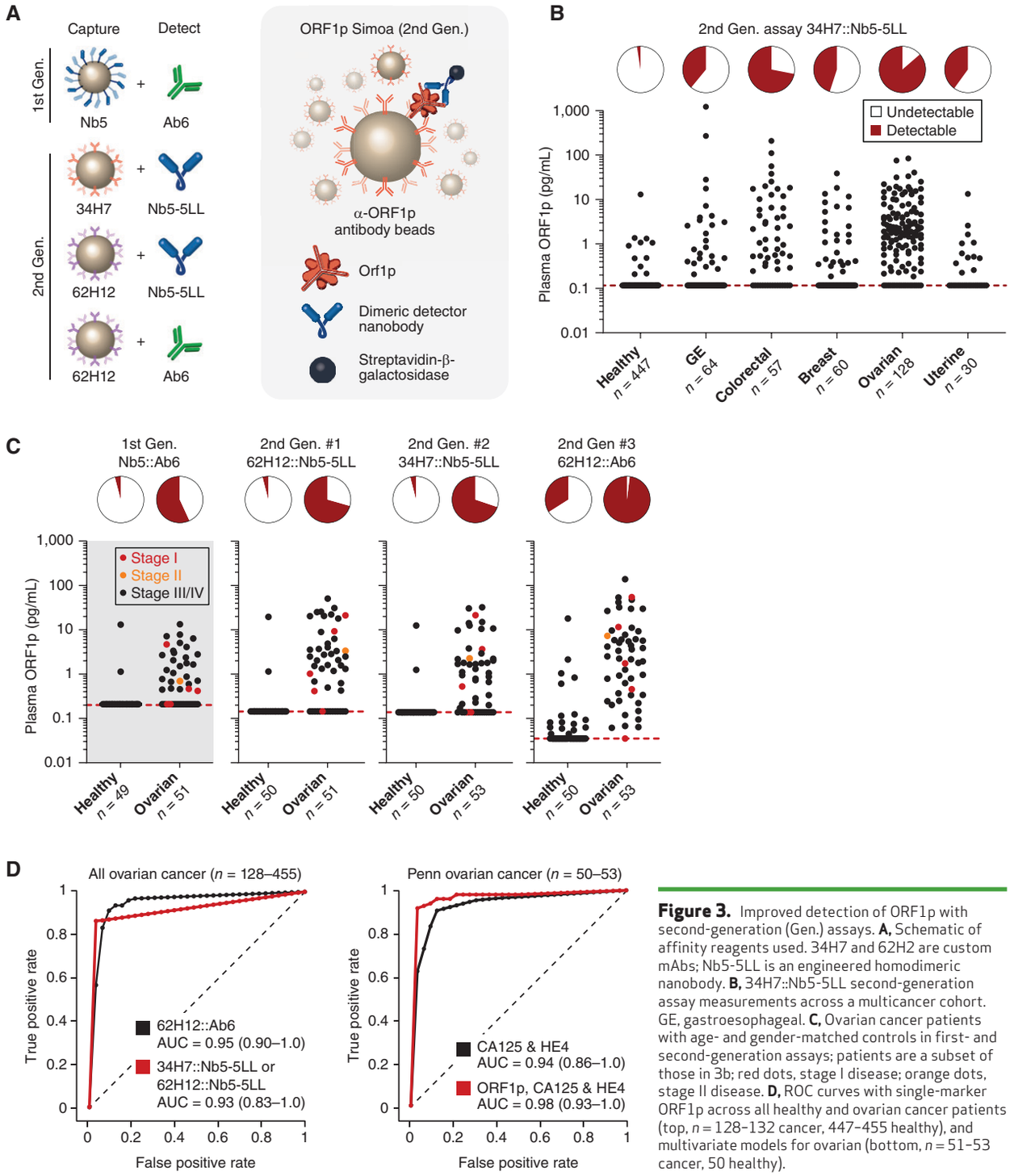

Figure 3. Improved detection of ORF1p with second-generation (Gen.) assays. **A,** Schematic of affinity reagents used. 34H7 and 62H2 are custom mAbs; Nb5-5LL is an engineered homodimeric nanobody. **B,** 34H7::Nb5-5LL second-generation assay measurements across a multicancer cohort. GE, gastroesophageal. **C,** Ovarian cancer patients with age- and gender-matched controls in first- and second-generation assays; patients are a subset of those in 3b; red dots, stage I disease; orange dots, stage II disease. **D,** ROC curves with single-marker ORF1p across all healthy and ovarian cancer patients (top, $n = 128$–132 cancer, 447–455 healthy), and multivariate models for ovarian (bottom, $n = 51$–53 cancer, 50 healthy).

alone, AUC = 0.94, 59% sensitivity at 98% specificity; ORF1p, CA125, and HE4, AUC = 0.98, 91% sensitivity at 98% specificity; Fig. 3D bottom panel, Supplementary Fig. S21; Supplementary Table S8). Although it is not clear whether the low ORF1p levels detected in several healthy individuals are due to nonspecific binding, true background levels of ORF1p, or an unappreciated premalignant state, several positive healthy controls were positive by only one of the three second-generation assays ($n = 4$ positive by only 62H12::Nb5-5LL and $n = 75$ positive by only 62H12:Ab6), suggesting nonspecific binding in at least some of these cases and the potential to improve specificity by combining data from multiple assays. Our results indicate that by developing improved affinity reagents, we achieved improved clinical sensitivity in detecting

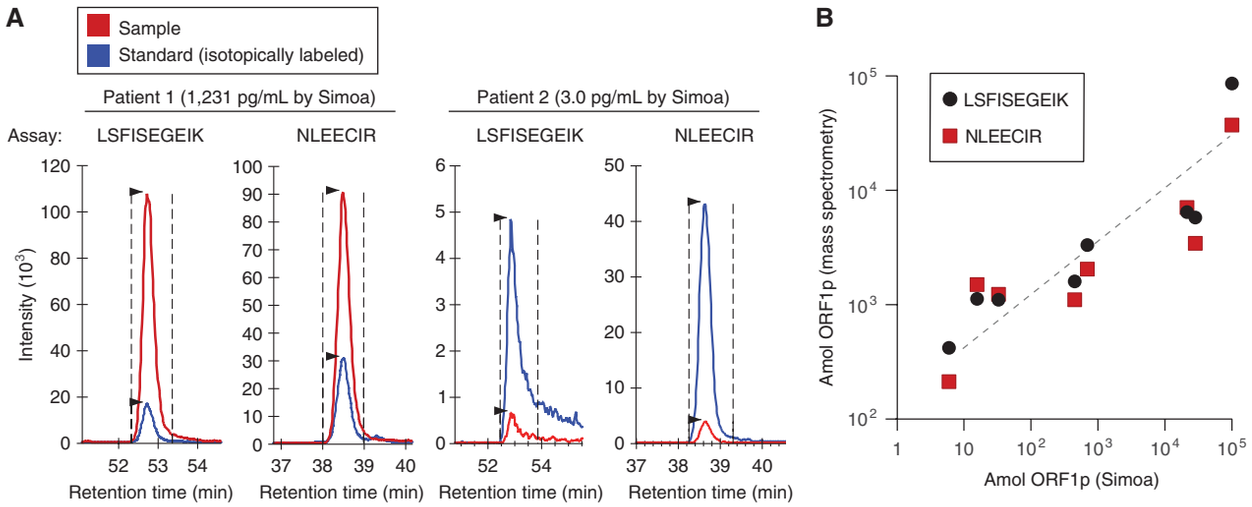

Figure 4. Targeted proteomics measurements of plasma ORF1p from large sample volumes. **A,** ORF1p measured from two gastric cancer patients using two quantotypic peptides (LSFISEGEIK and NLEECIR, red traces) with internal isotopically labeled standards (blue traces); a high-ORF1p cancer patient [1,231 pg/mL by Simoa, 3.5 mL plasma used for immunoprecipitation (IP)] and high-ORF1p healthy patient (3.0 pg/mL by Simoa, 5 mL plasma used for IP) are shown with 900 amol standard injected. **B,** Correlation between measured ORF1p by Simoa and targeted proteomics assays; $r = 0.97$ (Simoa vs. LSFISEGEIK) and $r = 0.99$ (Simoa vs. NLEECIR, t test), $P < 0.0001$ for both.

circulating ORF1p in cancer patients, with 83% sensitivity at >98% specificity toward early detection of ovarian cancer.

Receptor subtypes were available for the breast cancer cohort, which includes 30 patients each with metastatic and localized disease (Supplementary Fig. S22A and S22B). Across all assays, triple negative tended to have higher positivity rates, but the most sensitive second-generation assay (62H12::Ab6) detected 96% of triple-negative cases and 91% of the remaining cases (Supplementary Fig. S22) with 93% sensitivity for both localized and metastatic disease. Overall, metastatic disease was detected more commonly than localized disease (43% vs. 6.7% for first-generation assay, 67%–93% vs. 23%–93% for second-generation assays, depending on the assay), and all three second-generation assays had higher sensitivity than the first-generation assay (Supplementary Fig. S22).

To further validate our results, we developed a targeted proteomics approach to measure ORF1p following affinity capture, with two distinct peptides measured versus internal isotopically labeled control peptides (Fig. 4A). With this assay, we applied much larger volumes of plasma (3–6 mL, 120–240-fold more than the 25 μL used in Simoa assays) from a cohort of 10 patients, including 2 gastroesophageal (GE) cancer patients and one healthy control with very high ORF1p (230–1,230 pg/mL), two healthy controls with high ORF1p, (3–5 pg/mL), and 5 healthy controls with low ORF1p (undetectable: 0.2 pg/mL). The results (Fig. 4A and B; Supplementary Fig. S23A–S23D) show a strong correlation with Simoa, providing further confidence in our results ($r = 0.97$–0.99, $P < 0.0001$, t test).

Building on the improvements made through nanobody engineering in our second-generation assays, we developed an expanded set of homodimeric, heterodimeric, and heterotrimeric anti-ORF1p nanobodies and screened them in combination with 34H7 and 62H12 capture antibodies, resulting in "third-generation" assays (Supplementary Figs. S11, S14, S24, and S25). We noticed that reagents containing Nb2 performed very well in Surface Plasmon Resonance (SPR) but poorly in Simoa detection, and we hypothesized this was because Nb2 contains a lysine in the complementarity-determining region (CDR), which would be biotinylated in the procedure, reducing affinity. We therefore engineered the new reagents to be C-terminally biotinylated on cysteine residues and varied linker sequences. Five of these assays, which utilize Nb2- and Nb9-containing constructs, outperform our second-generation assays in a cohort of 25 GE cancer patients with ORF1p measurements that were mostly undetectable previously, while maintaining high specificity versus healthy individuals (Fig. 5A; Supplementary Fig. S25).

To leverage more sensitive assays for ORF1p detection, we next tested ORF1p affinity reagents from one of the second-generation Simoa assays on our recently developed Molecular On-bead Signal Amplification for Individual Counting platform (MOSAIC; Fig. 5B). MOSAIC develops localized on-bead signal from single captured molecules, in contrast to the microwell array format in Simoa, and improves analytical sensitivity by an order of magnitude over Simoa via increasing the number of beads counted (26). Furthermore, as the developed Simoa assays used only 25 μL plasma, we hypothesized that using larger plasma volumes would enhance ORF1p detectability by increasing the number of analyte molecules present. By using a 20-fold higher sample volume (500 μL plasma) and the MOSAIC platform, we achieved 10-fold higher analytical sensitivity, with a limit of detection of 0.002 pg/mL ORF1p (17 aM trimer; Supplementary Fig. S26). Indeed, in a pilot cohort of GE cancer and healthy patients, ORF1p levels in 9 of 10 previously undetectable cancer patients were readily discriminated from healthy individuals (Fig. 5C). Thus, in addition to improved affinity reagents, using larger sample volumes and more analytically sensitive technologies can further enhance both sensitivity and discrimination of circulating ORF1p levels

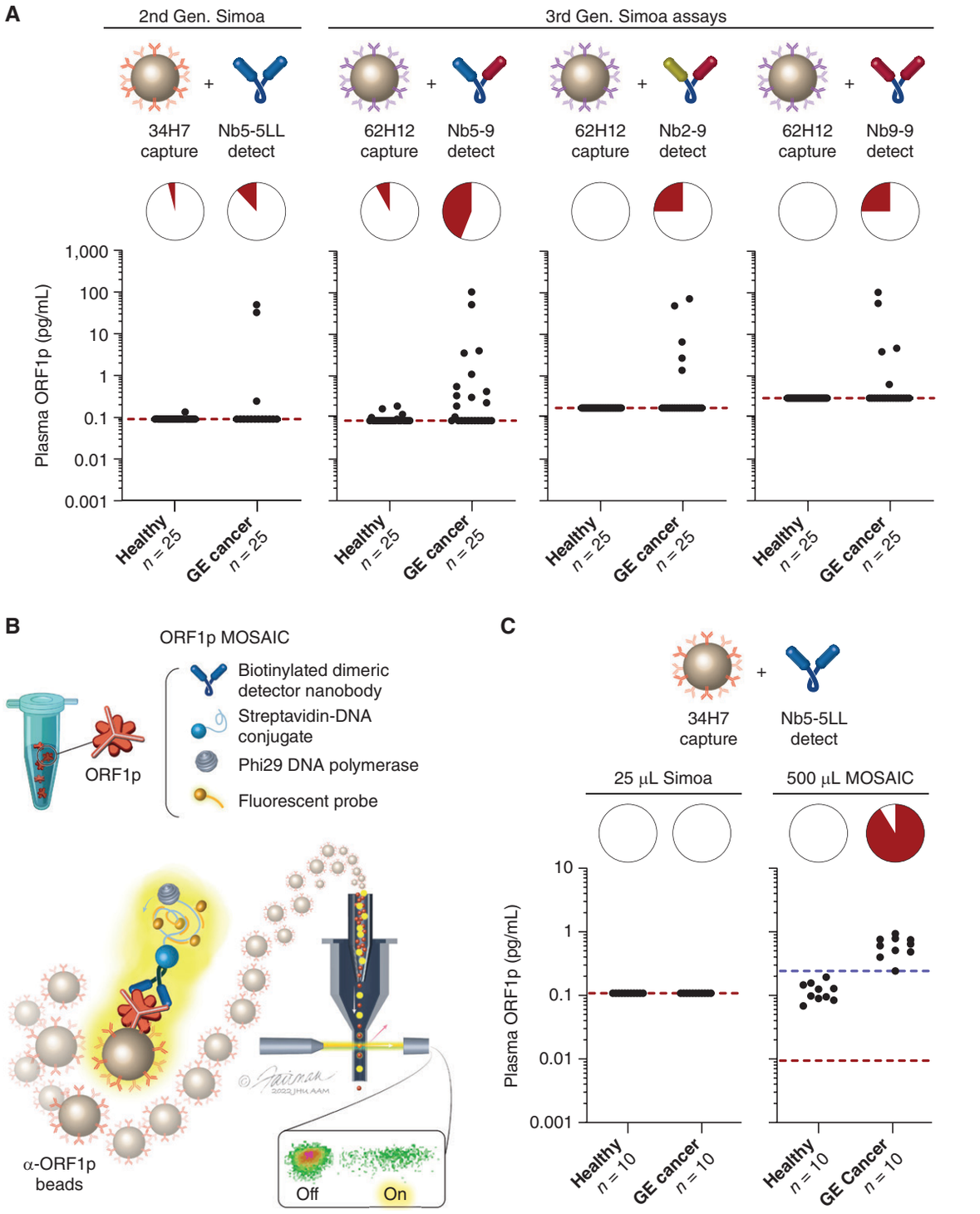

Figure 5. Improved detection of ORF1p with third-generation Simoa assays and with MOSAIC assays. **A,** Comparison of second- and third-generation Simoa assays (25 μL) in 25 mostly undetectable GE cancer and healthy control patients. **B,** Schematic of MOSAIC assays. Captured single-molecule "immunosandwiches" are formed analogously to Simoa assays. DNA-conjugated streptavidin enables rolling circle amplification to be carried out, generating a strong local fluorescent signal on the bead surface, and then "on" and "off" beads are quantified by flow cytometry, allowing efficient sampling of larger numbers of capture beads. This results in improved sensitivity and multiplexing capabilities. Illustration: Jennifer E. Fairman, CMI, FAMI. © 2023 Johns Hopkins University, AAM. **C,** 37H7::Nb5-5LL MOSAIC and Simoa assays in 10 previously undetectable GE cancer and healthy control patients. Red dashed lines indicate the analytical limit of detection for recombinant ORF1p in the buffer. Blue dashed line in **C** indicates plasma-specific background in large-volume MOSAIC assays, which is used to determine positivity in the pie charts.

between healthy controls and patients with cancer. The relative contributions of increased volume and the improved assay platform to the increased sensitivity remain to be explored; the assay background seen in patient plasma (blue dashed line) but not in buffer (analytical limit of detection, red dashed line) will also require further optimization.

To test whether ORF1p might be useful for monitoring therapeutic response, 19 patients with GE cancer were identified who had both detectable plasma ORF1p at diagnosis as well as subsequent samples available collected during or after treatment (average 80 days after initiation of therapy; range, 26–179 days). Primary tumors were all adenocarcinoma and located in the esophagus (n = 7), GE junction (n = 7), and stomach (n = 5). All patients received systemic therapy. A smaller fraction of patients also received radiation and/or surgery (Supplementary Table S9). Clinical response (responders and nonresponders) was determined by a review of restaging CT and PET-CT imaging by clinicians blinded to the assay results. Over an average of 465 days (range, 98–1,098), 12 patients died, 6 were alive at the last follow-up (all responders), and 1 was lost to follow-up. Nonresponders had higher pretreatment plasma ORF1p (Fig. 6A, left, P = 0.02). All 6 patients with detectable ORF1p at follow-up sampling, as defined by positivity over background in two of three assays, were also nonresponders by imaging (Fig. 6A, right, $P < 0.0001$, Fisher Exact test) and had reduced survival (P = 0.001 log-rank test for overall survival). In contrast, in all 13 responders, circulating ORF1p dropped to undetectable levels at follow-up sampling. Plasma ORF1p in four responders and two nonresponders was measured at an early time point of 26 to 33 days. The timing of sampling was not different between groups (average 93 days for nonresponders, 74 for responders, P = 0.5). Pretherapy blood was drawn on an average of 20 days after diagnosis (range, -8–48; average 22 for nonresponders and 19 for Responders, P = 0.6). Representative PET and PET-CT images are shown (Fig. 6B), both images are taken approximately two months after initiation of therapy, a month after the plasma ORF1p result. Thus, reduction in circulating ORF1p paralleled treatment response and survival, while persistent circulating ORF1p corresponded to patients with refractory disease, indicating the predictive potential of this marker.

Because these results indicated that pretreatment plasma ORF1p levels might be prognostic, we evaluated the prognostic value of second-generation ORF1p Simoa assays in our cohorts of GE, colorectal cancer, and ovarian cancer patients. We stratified the patients based on either the median ORF1p value or ORF1p detectability (methods) and found that higher pretherapy plasma ORF1p was significantly associated with poor survival in GE and colorectal cancer (Fig. 6C; Supplementary Fig. S27, P = 0.0017 and 0.011, log-rank test, respectively) but not in ovarian cancer (Supplementary Fig. S27). ORF1p remained significantly prognostic in multivariate analysis in GE and colorectal cancer (Methods; Supplementary Figs. S28 and S29; Supplementary Tables S10 and S11).

DISCUSSION

Taken together, our data reveal for the first time that circulating ORF1p is a multicancer protein biomarker with potential utility across clinical paradigms, including early detection, risk stratification, prognostication, and treatment response. These assays are enabled by ultrasensitive single-molecule detection technologies and high-quality affinity reagents, which are both required due to the attomolar-to-femtomolar circulating levels of ORF1p in cancer patients. Iterative improvements including optimized affinity reagents, buffer, and assay design yield highly sensitive and specific assays. A 20-fold volume scale-up to 500 μL appears promising for improving sensitivity without obviously compromising specificity, and this volume remains much smaller than a typical 5 to 10 mL blood draw and could be scaled further without limiting clinical applicability, although it remains unclear how much of this improvement was due to the increased volume or the MOSAIC platform itself; future studies are needed to address the relative contributions to sensitivity by sample volume and platform. The data strongly suggest that these assays are measuring *bona fide* tumor-derived circulating ORF1p for the following reasons: (i) four developed assays with predominantly nonoverlapping high-affinity reagents all measure similar levels across hundreds of samples; (ii) levels appear specific to cancer patients, whose tumors overexpress ORF1p; (iii) they correlate strongly with measurements made by targeted proteomics; and (iv) plasma levels pretreatment and on/posttreatment correlated with therapeutic response. Nonetheless, the low levels of circulating ORF1p make orthogonal confirmation in larger cohorts by any other method challenging, as even the most sensitive mass spectrometry assays have limits of detection orders of magnitude higher.

The results expand our understanding that L1 expression is early and pervasive across carcinomas from multiple organs and high-risk precursor lesions, including dysplastic BE, which is challenging to diagnose and manage. Circulating ORF1p shows promise in early detection applications and may be more useful as part of a multianalyte detection test combined with, for example, cfDNA methylation, longitudinal CA125 in ovarian cancer, or CEA in colorectal cancer (3, 5, 27). We demonstrate that ORF1p is an early indicator of chemotherapeutic response in gastric and esophageal cancers at time points as short as 26 days, where other parameters are often ambiguous, opening possibilities for monitoring minimal residual disease or relapse. Shorter time intervals will be needed to understand whether ORF1p can monitor tumor lysis. Importantly, ORF1p appears to provide a level of specificity for cancers not achieved by other protein biomarkers, likely due to the unique biology of the retrotransposon, with repression of L1 in normal somatic tissue (9, 13, 14). ORF1p is therefore attractive as a putative binary cancer biomarker, in which a positive signal is highly specific for disease, with diagnostic utility both in tissue and plasma.

The assays are cost-effective (<$3 in consumables), rapid (<2 hours), simple to perform, scalable, and have clinical-grade coefficients of variation (<15%). Flow cytometers for MOSAIC are common in clinical reference laboratories, and the assay could be modified for DNA-based readout by qPCR or sequencing. Limitations of the current work include the relatively small numbers of early-stage samples, a small and heterogeneous GE therapeutic cohort, and relatively small,

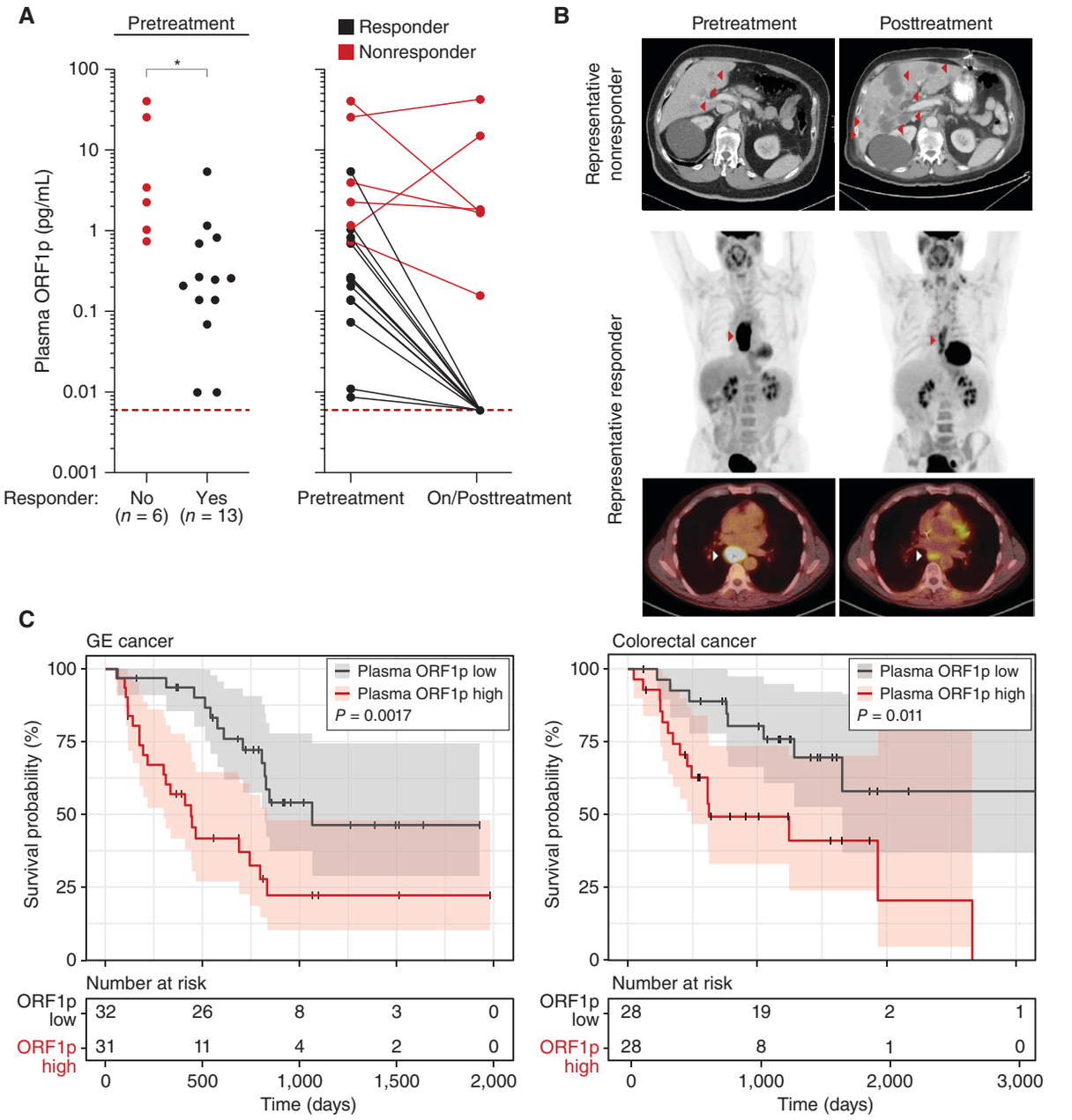

Figure 6. ORF1p is an early predictor of response in 19 GE patients undergoing chemo/chemoradiotherapy and is prognostic in GE and colorectal cancers (CRC). Responders and nonresponders were characterized retrospectively by medical oncologists blinded to the assay results by post-therapy and presurgery imaging. **A,** Plasma ORF1p as measured by all three second-generation Simoa assays before and during/posttreatment; left, nonresponders have higher pretreatment ORF1p than responders ($P = 0.02$, t test); right, ORF1p pretherapy and on/posttherapy classifies responders and nonresponders; $P < 0.0001$, Fisher exact test. **B,** Representative CT and PET-CT from patients in the cohort. The representative nonresponder has the second-highest plasma ORF1p pretreatment (25.8 pg/mL), which increased to 43.0 pg/mL at day 28 of FOLFOX therapy (47 days after diagnosis), concomitant with increased sizes and number of hepatic metastases seen on CT at day 61. The representative responder has the fourth-highest plasma ORF1p value in the cohort of responders (0.83 pg/mL), which decreased to undetectable at day 26 of CROSS therapy (48 days after diagnosis); the displayed PET-CT is 59 days after initiation of therapy, 31 days after the second ORF1p measurement. **C,** Kaplan–Meier survival analysis of patients categorized as plasma ORF1p-high and ORF1p-low based on the median plasma ORF1p assay value shows significantly longer survival for ORF1p-low patients with GE (stages III–IV, $P = 0.0017$, log-rank test) and colorectal cancer (all stage IV, $P = 0.011$, log-rank test). Shaded regions represent 95% confidence intervals.

heterogeneous, and mostly late-stage cohorts in survival analysis. Larger cohorts will be needed for further validation. The results are limited thus far to carcinomas; hematologic, mesenchymal, skin, and central nervous system cancers have not yet been studied. Further optimizations to both assay design and reagents will likely be possible, and larger cohorts are needed to further validate and develop third-generation Simoa assays and improved MOSAIC assays,

including automation of MOSAIC for scalability. Finally, it is unclear how ORF1p, which is normally cytosolic, enters the blood and what clinicopathologic factors might affect these levels. Although senescent and germ cells in humans and mice are known to produce ORF1p (28–30), they may release ORF1p differently than tumor cells or may not release appreciable ORF1p at all. Arguing against significant release from senescent or germ cells, there was no correlation of plasma ORF1p with age or sex in either healthy or cancer patient samples. Future work will also be needed to understand whether there is a normal baseline level of circulating ORF1p, as implied by the trace amounts seen when ORF1p was measured from much larger volumes of plasma using targeted mass spectrometry, and what factors affect this level.

METHODS

Materials

All affinity reagents used in this work are listed in Supplementary Table S2. Conjugation reagents, paramagnetic beads, and assay buffers were obtained from Quanterix Corporation. DNA oligos used in the MOSAIC assay were obtained from Integrated DNA Technologies. Antibodies used in final Simoa and MOSAIC assays (monoclonals Ab6, Ab54, 62H12, and 34H7) were additionally validated by western blotting (Supplementary Fig. S15).

Preparation of Capture and Detector Reagents

All capture antibodies and nanobodies were obtained in or dialyzed into phosphate-buffered saline (PBS). For the first-generation Simoa assay, 7×10^8 carboxylated paramagnetic 2.7-μm beads (Homebrew Singleplex Beads, Quanterix Corp.) were first washed three times with 400 μL Bead Wash Buffer (Quanterix Corp.) and two times with 400 μL cold Bead Conjugation Buffer (Quanterix Corp.) before being resuspended in 390 μL cold Bead Conjugation Buffer. A 1-mg vial of 1-ethyl-3-(3-dimethylaminopropyl) carbodiimide hydrochloride (EDC; Thermo Fisher Scientific) was then dissolved to 10 mg/mL in cold Bead Conjugation Buffer, and 10 μL was added to the beads. The beads were shaken for 30 minutes at 4°C to activate the carboxyl groups on the beads, which were then washed once with 400 μL cold Bead Conjugation Buffer and resuspended in the capture nanobody solution (10 μg nanobody total), diluted in Bead Conjugation Buffer to a final volume of 400 μL. The beads were shaken for two hours at 4°C, washed twice with 400 μL Bead Wash Buffer, and resuspended in 400 μL Bead Blocking Buffer (Quanterix Corp.) before shaking at room temperature for 30 minutes to block the beads. After one wash each with 400 μL Bead Wash Buffer and Bead Diluent (Quanterix Corp.), the beads were resuspended in Bead Diluent and stored at 4°C. Beads were counted with a Beckman Counter Z Series Particle Counter before using in assays. For second-generation Simoa assays, the following bead coupling conditions were used: 4.2×10^8 starting beads, 300 μL wash volumes, 6 μL EDC, and 40 μg antibody.

For biotinylation of detector antibodies or nanobodies, a 1-mg vial of Sulfo-NHS-LC-LC-biotin was freshly dissolved in 150 μL water and added at 80-fold molar excess to a 1 mg/mL solution of antibody or nanobody. The reaction mixture was incubated for 30 minutes at room temperature and subsequently purified with an Amicon Ultra-0.5 mL centrifugal filter (50K and 10K cutoffs for antibody and dimeric nanobody, respectively). Five centrifugation cycles of 14,000 ×*g* for five minutes were performed, with the addition of 450 μL PBS each cycle. The purified biotinylated detector reagent was recovered by inverting the filter into a new tube and centrifuging at 1,000 ×*g* for two minutes. Concentration was quantified using a NanoDrop spectrophotometer.

Recombinant ORF1p Protein Production

ORF1p was prepared as described (25); briefly, codon-optimized human ORF1p corresponding to L1RP (L1 insertion in X-linked retinitis pigmentosa locus, GenBank AF148856.1) with N-terminal His6-TEV was expressed in *E. coli*, purified by Ni-NTA affinity, eluted, tag cleaved in the presence of RNaseA, and polished by size exclusion in a buffer containing 50 mmol/L HEPES pH 7.8, 500 mmol/L NaCl, 10 mmol/L MgCl2, and 0.5 mmol/L tris(2-carboxyethyl) phosphine (TCEP), resulting in monodisperse trimeric ORF1p bearing an N-terminal glycine scar.

Nanobody Generation and Screening

Nanobodies were generated essentially as described (31, 32) using mass spectrometry/lymphocyte cDNA sequencing to identify antigen-specific nanobody candidates. Briefly, a llama was immunized with monodisperse ORF1p, and serum and bone marrow were isolated. The heavy chain-only IgG fraction (VHH) was isolated from serum and bound to a column of immobilized ORF1p. Bound protein was eluted in SDS and sequenced by mass spectrometry, utilizing a library derived from sequencing VHH fragments PCR-amplified from bone marrow–derived plasma cells. Candidate sequences were cloned into an *E. coli* expression vector with C-terminal His6 tag and expressed in 50 mL cultures in *E. coli* Arctic Express RP (Agilent) with 0.2 mmol/L IPTG induction at 12°C overnight. Periplasmic extract was generated as follows: pellets were resuspended in 10 mL per L culture Tris EDTA and sucrose (TES) buffer (200 mmol/L Tris-HCl, pH 8.0, 0.5 mmol/L EDTA, and 500 mmol/L sucrose), 20 mL/L hypotonic lysis buffer added (TES buffer diluted 1:4 with ddH_2O), supplemented with 1 mmol/L PMSF, 3 μg/mL Pepstatin A, incubated 45 minutes at 4°C, and centrifuged at 25,000 × g for 30 minutes. The supernatant (periplasmic extract) was bound to ORF1p-conjugated Sepharose, washed 3 times, eluted with SDS at 70°C for 10 minutes, and periplasmic extract and elution were analyzed by SDS-PAGE to assay expression and yield. ORF1p-binding candidates were purified as below and analyzed by ELISA (Supplementary Fig. S7).

Nanobody and Multimeric Nanobody Purification

C-terminally His6-tagged nanobody constructs were expressed and purified essentially as described (31). Briefly, protein was expressed in *E. coli* Arctic Express RP (Agilent) with 0.2 mmol/L IPTG induction at 12°C overnight. Periplasmic extract (generated as above) was supplemented with 5 mmol/L $MgCl_2$, 500 mmol/L NaCl, and 20 mmol/L imidazole, purified by Ni-NTA chromatography, dialyzed into 150 mmol/L NaCl, 10 mmol/L HEPES, pH 7.4, and concentrated to 1 to 3 mg/mL by ultrafiltration. "5xCys tail" constructs were purified with the addition of 5 mmol/L TCEP-HCl in resuspension, wash, elution, and dialysis buffers.

SPR Assays

Binding kinetics (k_a, k_d, and K_D) of antibody and nanobody constructs for ORF1p were obtained on a Biacore 8K instrument (Cytiva). Recombinant ORF1p was immobilized on a Series S CM5 sensor chip at 1.5 μg/mL using EDC/NHS coupling chemistry according to the manufacturer's guidelines. Nanobodies and antibodies were prepared as analytes and run in buffer containing 20 mmol/L HEPES pH 7.4, 150 mmol/L NaCl, and 0.05% Tween-20. Analytes were injected at 30 μL/minute in single-cycle kinetics experiments at concentrations of 0.1, 0.3, 1, 3.3, and 10 nmol/L, with association times of 120 to 180 seconds, and a dissociation time of 1,200 to 7,200 seconds, depending on observed off-rate. Residual-bound protein was removed between experiments using 10 mmol/L glycine-HCl pH 3.0. Data were analyzed using Biacore software, fitting a Langmuir 1:1 binding model to sensorgrams to calculate kinetic parameters.

For epitope binning, pairs of antibodies were sequentially flowed over immobilized ORF1p using Biacore tandem dual injections

according to the manufacturer's guidelines. Antibodies were injected at concentrations of 200 nmol/L with a flow rate of 10 μL/minute. Contact time for the first antibody was 120 seconds, followed by 150 seconds for the second antibody, then a 30-second dissociation. Response signal for the second antibody was measured in a 10-second window at the beginning of dissociation. The chip was regenerated between experiments with glycine pH 3.0 as above. Data were analyzed using the Biacore software epitope binning module.

ORF1p Simoa Assays

Simoa assays were performed on an HD-X Analyzer (Quanterix Corp.), with all assay reagents and consumables loaded onto the instrument according to the manufacturer's instructions. 250,000 capture beads and 250,000 helper (nonconjugated) beads were used in each Simoa assay. A three-step assay configuration was used for the first- and second-generation assays, consisting of a 15-minute target capture step (incubation of capture beads with 100 μL sample), 5-minute incubation with detector reagent (0.3 μg/mL for both first- and second-generation assays), and 5-minute incubation with streptavidin-β-galactosidase (150 pmol/L for first-generation assay; 300 pmol/L for second-generation assays). The beads were washed with System Wash Buffer 1 (Quanterix Corp.) after each assay step. Upon the final wash cycle, the beads were loaded together with the fluorogenic enzyme substrate resorufin β-D-galactopyranoside into a 216,000-microwell array, which was subsequently sealed with oil. Automated imaging and counting of "on" and "off" wells and calculation of average enzyme per bead were performed by the instrument. Calibration curves were fit using a 4PL fit with a $1/y^2$ weighting factor, and the limit of detection (LoD) was determined as three standard deviations above the blank.

All plasma and serum samples were diluted 4-fold in Homebrew Sample Diluent (Quanterix Corp.) with 1x Halt Protease Inhibitor Cocktail (Thermo Fisher), with an additional 1% Triton X 100 added in the second-generation assays. All recombinant ORF1p calibrators were run in triplicates, with four replicates for the blank calibrator, and all plasma and serum samples were run in duplicates. The average LoD across all sample runs was determined for each assay and depicted in each figure.

Healthy individual plasma and serum samples were obtained from the Mass General Brigham Biobank, with additional samples from the Penn Ovarian Cancer Research Center and Tomas Mustelin (University of Washington). Additional breakdown of patients within each cancer type, by demographic and clinicopathologic variables, where available, is included in Supplementary Figs. S2, S3, S7, S8, and S22, and Supplementary Table S12.

ORF1p Large-Volume MOSAIC Assays

MOSAIC assays were performed as previously described, using 2 mL microcentrifuge tubes for the initial capture step. For each sample, 500 μL plasma was diluted 4-fold in Homebrew Sample Diluent with protease inhibitor and 1% Triton X 100 to a total volume of 2 mL. Briefly, 100,000 capture beads were incubated with a sample and mixed for 2 hours at room temperature, followed by magnetic separation and resuspended in 250 μL System Wash Buffer 1 before transferring to a 96-well plate. The beads were then washed with System Wash Buffer 1 using a Biotek 405 TS Microplate Washer before adding 100 μL nanobody detector reagent (0.3 μg/mL, diluted in Homebrew Sample Diluent) and shaking the plate for 10 minutes at room temperature. After washing with the microplate washer, the beads were incubated with 100 μL streptavidin-DNA (100 pmol/L, diluted in Homebrew Sample Diluent with 5 mmol/L EDTA and 0.02 mg/mL heparin) with shaking for 10 minutes at room temperature, followed by another washing step. The beads were transferred to a new 96-well plate, manually washed with 180 μL System Wash Buffer 1, and resuspended in 50 μL reaction mixture for rolling circle amplification (RCA). The RCA reaction mixture consisted of 0.33 U/μL phi29 polymerase, 1 nmol/L ATTO647N-labeled DNA probe, 0.5 mmol/L deoxyribonucleotide mix, 0.2 mg/mL bovine serum albumin, and 0.1% Tween-20 in 50 mmol/L Tris-HCl (pH 7.5), 10 mmol/L $(NH_4)_2SO_4$, and 10 mmol/L $MgCl_2$. The beads were shaken at 37°C for one hour, followed by the addition of 160 μL PBS with 5 mmol/L EDTA and 0.1% Tween-20. After washing the beads once with 200 μL of the same buffer, the beads were resuspended in 140 μL buffer with 0.2% BSA. All samples were analyzed using a NovoCyte flow cytometer (Agilent) equipped with three lasers. Analysis of average molecule per bead values was performed as previously described using FlowJo software (BD Biosciences) and Python. All code used for MOSAIC data analysis can be downloaded as part of the waltlabtools.mosaic Python module, which is available at https://github.com/tylerdougan/waltlabtools.

Targeted Proteomics Analysis of Immunoprecipitated ORF1p

Protein levels of the LINE-1 ORF1p (UniProt ID: Q9UN81) were determined with targeted proteomics using isotopically labeled standard peptides (AQUA QuantProHeavy peptides with $^{13}C^{15}N$-labeled C-terminal lysine or arginine; Thermo Fisher) for accurate quantification. Assays were developed for two quantotypic peptides of ORF1p, namely, LSFISEGEIK and cysteine-alkylated NLEECITR (the approach is similar to the assay development described previously for other proteins (33)). Briefly, 3–6 mL patient plasma was diluted with an equal volume of 2× dilution buffer (PBS containing 2% Triton X-100, 10 mmol/L EDTA, and 1 Pierce protease inhibitor tablet per 25 mL (2× concentration, Thermo) for a final concentration of 1% Triton X-100, 5 mmol/L EDTA, and 1× protease inhibitor and bound to 7 million 62H12-conjugated magnetic beads for 1 hour at room temperature. Beads were washed 3 times with 5× PBS containing 0.1% tween 20 and 1× protease inhibitor, then once with the same buffer lacking tween 20, and eluted in 50 μL buffer containing 2% SDS and 50 mmol/L Tris pH 8.5 by heating for 5 minutes at 95°C with agitation. Separated eluates were subjected to in-gel digestion using trypsin (150 ng sequencing grade modified trypsin V5111; Promega) after reduction with 10 mmol/L dithiothreitol and alkylation with 55 mmol/L iodoacetamide proteins, prior to LC-MS analyses of the target peptides (33).

Classification Models

Classification models were trained for all healthy and all ovarian cancer patients measured by the second-generation assays; and the subset of 51 ovarian cancer and 50 age-matched healthy female patients, obtained from Ronny Drapkin (University of Pennsylvania). Each data set contained no missing values, and the measurements in the data sets were log-transformed and normalized beforehand for classification analysis of healthy and ovarian cancer subjects. Logistic regression was used for the univariate classifier and the k-nearest neighbors and light gradient-boosting machine (LightGBM), which had the best performances among the classifiers, were used for the multivariate classifier, and implemented in Python 3.7.15 with scikit-learn version 1.0.2 package. Each classifier was given a weight optimization between classes to deal with data imbalance between healthy and cancer subjects, as well as hyperparameter tuning using grid search.

The performance of each biomarker in differentiating ovarian cancer subjects from healthy subjects was evaluated with 5-fold cross-validation by calculating accuracy, precision, recall, f1-value, sensitivity, specificity, and area under the receiver-operating characteristic (ROC) curve (AUC). A stratified 5-fold cross-validation strategy randomly splits the positive and negative samples into five equally sized subsets. One positive subset and one negative subset were selected as

the test data set each time, and the other samples were used to train a classification model.

In the multivariate analysis, the variance inflation factor (VIF) for the biomarkers was calculated, and any biomarkers with extremely high correlation with VIF greater than 10 were excluded from the classification model in advance.

BE Cases

A cohort of 75 esophageal biopsies with BE and varying degrees of dysplasia were assembled. Negative cases were screened to have no prior history of dysplasia. The mean age of the cohort was 67 years with a male predominance (M:F ratio = 3.7:1). All samples were reanalyzed for histologic features of dysplasia by three experienced gastrointestinal pathologists (LRZ, VD, and OHY) who were blinded to the original diagnosis. A consensus was reached for 72 cases, and the consensus diagnosis was used as the gold standard. There was moderate agreement between pathologists (kappa 0.43–0.51).

Colon Cancer Tissue Microarray

A total of 178 sequential colorectal cancers resected by a single surgeon from 2011 to 2013 were assembled on a 3-mm core tissue microarray. All cases were independently scored by two pathologists. The mean age of the cohort was 65 years with 49.8% males. The mean follow-up was 25 months. At resection, 23% were stage I, 33% were stage II, 44% were stage III, and 1% were stage IV.

Ovarian Cancer Samples

Age-matched ovarian cancer (n = 53) and healthy control (n = 50) patient plasma samples were from the University of Pennsylvania Ovarian Cancer Research Center, OCRC Tumor BioTrust Collection, Research Resource Identifier (RRID): SCR_02287.

GE Cancer Treatment Cohort

Nineteen patients received systemic therapy, three of which also underwent surgical resection. Patients were treated with concurrent chemotherapy (carboplatin/taxol) and radiation (N = 3), fluorouracil/leucovorin/oxaliplatin/docetaxel (FLOT, N = 2), fluorouracil/leucovorin/irinotecan/oxaliplatin (FOLFIRINOX, N = 2), fluorouracil/leucovorin/oxaliplatin (FOLFOX, N = 9), FOLFOX + trastuzumab (N = 1), pembrolizumab (N = 1), or FOLFOX and then chemoradiation (1). The mean age of the cohort was 76 years. All patients were male (100%). Fifty-eight percent had locally advanced disease (stage II–III) and 42% had advanced disease (stage IV) at the time of initial diagnosis. Sixty-eight percent (N = 13) were deemed responders to therapy while 32% (N = 6) were deemed nonresponders to standard therapy on review of restaging imaging (CT and/or PET-CT) by investigators blinded to the assay results. Note that the on/posttreatment blood draw measured by Simoa often preceded these imaging studies.

Patient Consent

All plasma samples were obtained with informed written consent under IRB-approved protocols at Mass General Brigham (MGB), the University of Pennsylvania, and the University of Washington. All experiments with patient samples were conducted under IRB approval and in accordance with ethical guidelines in the Belmont Report. Tissue samples were obtained with consent, or, where appropriate, with waiver of consent under MGB-approved protocols.

Histochemistry. ORF1p IHC was performed essentially as described using anti-ORF1 4H1 (Millipore; 8) diluted 1:3,000 and reoptimized on a Leica Bond system (17). Cases were scored by three experienced gastrointestinal pathologists (MST, VD, and OHY) at two institutions. LINE-1 *in situ* hybridization was performed as described using RNAscope catalog 565098 (Advanced Cell Diagnostics) on a Leica Bond system (17). The probe is complementary to the 5′ end of L1RP (L1 insertion in X-linked retinitis pigmentosa locus). Cases were scored by three experienced gastrointestinal pathologists (MST, VD, and OHY).

Survival Analysis. Kaplan–Meier (KM) curves (34) were computed to study the association between overall survival and plasma ORF1p concentration in ovarian cancer, colorectal cancer, and esophageal cancer. To investigate the association with survival, we classified ORF1p concentrations in two different ways. First, by classifying each of the three assays as positive if the signal was above the LoD- in at least two out of three assays (majority vote method). Second, we evaluated whether ORF1p concentration measured by the most sensitive assay (62H12::Ab6) alone was associated with survival, classifying patients as ORF1p High and Low based on the cohort-specific median. The time variable was defined as days after diagnosis (GE and colorectal cancer) or treatment start (ovarian). Living patients were censored at the date of the last assessment. Because age at diagnosis was significantly associated with poor prognosis in colorectal cancer and male sex was significantly associated with a poor prognosis in GE cancer, we applied a Cox proportional hazards regression model (35); ORF1p was found to be independently prognostic (Supplementary Tables S10 and S11). Survival objects and KM curves were computed using the survival, ggpubr, and survminer packages in R. All tests were performed using R version 4.3.1 (The R Project for Statistical Computing, https://www.R-project.org/). The proportional hazard assumption was tested by plotting the Schoenfeld residuals and applying the Grambsch–Therneau test using the ggcoxdiagnostics function in R. The effect of influential observations was assessed by plotting the Deviance residuals using the ggcoxdiagnostics function in R. Original data for survival are provided in the "Supplementary Original Survival Data" file

Data Availability

Data were generated by the authors and included in the article and its supplementary data files. Survival and related assay data are provided in a supplementary file.

Authors' Disclosures

M.S. Taylor reports personal fees and other support from Rome Therapeutics and personal fees from Tessera Therapeutics outside the submitted work; in addition, M.S. Taylor has a patent for Application 63/423,696 pending. C. Wu reports other support from Quanterix Corporation outside the submitted work; in addition, C. Wu has a patent for Ultrasensitive Assays for the Detection of ORF1p in Biofluids pending to none. P.C. Fridy reports a patent for Ultrasensitive Assays for the Detection of ORF1p in Biofluids pending. L. Cohen reports a patent for 63/423,696 pending. K.R. Molloy reports a patent for 63/423,696 pending. B.T. Chait reports a patent for 63/423,696 pending. J.W. Franses reports grants and personal fees from Genentech, personal fees from Foundation Medicine, Eisai, and Servier outside the submitted work. M. Taplin reports other support from Janssen and Pfizer during the conduct of the study. M. Meyerson reports grants and other support from Bayer, grants from Janssen, Ono, personal fees from Interline, Isabl, Delve Bio, and other support from LabCorp outside the submitted work. R. Uppaluri reports personal fees from Merck, Inc, Daichi-Sankyo, and Regeneron outside the submitted work. L.M. Spring reports consultant/advisory board: Novartis, Puma, G1 therapeutics, Daiichi Pharma, Astra Zeneca, Eli Lilly; institutional research support: Merck, Genentech, Gilead, Eli Lilly. I. Shih reports grants from NIH during the conduct of the study. L. Pappas reports no relationships or activities that would have affected or potentially affected or influenced this work. However, Pappas reports equity (stock) ownership in Eli Lilly and Co. A.R. Parikh reports Equity in C2i Genomics XGenomes Cadex and

Parithera and in the last 36 months, has served as an advisor/consultant for Eli Lilly, Pfizer, Inivata, Biofidelity, Checkmate Pharmaceuticals, FMI, Guardant, AbbVie, Bayer, Delcath, Taiho, CVS, Value Analytics Lab, Seagen, Saga, AZ, Scare Inc, Illumina, Taiho, Hookipa and Science For America. She receives fees from Up to Date. She has received travel fees from Karkinos Healthcare. She has been on the DSMC for a Roche study and on Steering Committee for Exilixis. She has received research funding for the Institution from PureTech, PMV Pharmaceuticals, Plexxicon, Takeda, BMS, Mirati, Novartis, Erasca, Genentech, Daiichi-Sankyo, and Syndax. R.B. Corcoran reports other support from Alterome Therapeutics, Sidewinder Therapeutics, C4 Therapeutics, Avidity Biosciences, Cogent Biosciences, Erasca, Nested Therapeutics, Interline Therapeutics, nRichDx, Kinnate Biopharma, Remix Therapeutics, Revolution Medicines, Theonys, grants from Lilly, Novartis, Pfizer, personal fees from AbbVie, Array Biopharma, Astex Pharmaceuticals, Asana Biosciences, BMS, C4 Therapeutics, Cogent Biosciences, Elicio, FOG Pharma, Guardant Health, Ipsen, Kinnate Biopharma, Mirati Therapeutics, Navire, Nested Therapeutics, N-of-One, nRichDx, Remix Therapeutics, Revolution Medicines, Roivant, Syndax, Taiho, Tango Therapeutics, Theonys, Zikani Therapeutics, and Natera outside the submitted work. T. Mustelin reports personal fees from Rome Therapeutics and Bristol Myers Squibb outside the submitted work. Ömer H. Yilmaz reports personal fees from Ava Life Science, AI Protein and Nestle Health Sciences, grants from Microbial Machines outside the submitted work. U.A. Matulonis reports personal fees from Allarity, GSK, Profound Bio, Eisai, Agenus, Alkermes, Symphogen, Immunogenicity, Ovarian Cancer Research Alliance, Next Cure, Trillium, Novartis, Boerhinger Ingelheim, Morphosys, CureLab, Med Learning Group, GSK, Merck, and Pfizer outside the submitted work. A. Chan reports personal fees from Boehringer Ingelheim, grants and personal fees from Pfizer Inc., grants from Zoe Ltd, grants from Freenome, outside the submitted work. S.J. Skates reports grants from NCI (CA152990 and CA271871) during the conduct of the study; Guardant Health and other support from SISCAPA Assay Technologies outside the submitted work. B.R. Rueda reports grants from Nile Albright Research Foundation, Vincent Memorial Research Foundation, and P30CA006516 during the conduct of the study; other support from VincenTech outside the submitted work. R. Drapkin reports grants from NCI P50 SPORE in ovarian cancer, the Department of Defense, Gray Foundation, and Canary Foundation during the conduct of the study; personal fees and other support from Repare Therapeutics and other support from VOC Health, Inc outside the submitted work; in addition, R. Drapkin has a patent for methods for detecting ovarian cancer issued. S.J. Klempner reports personal fees from Astellas, Amgen, Merck, Sanofi-Aventis, BMS, AstraZeneca, Daiichi-Sankyo, Novartis, Pfizer, Servier, Coherus, Exact Sciences, Eli Lilly, Natera, other support from TP Therapeutics, and Nuvalent outside the submitted work. D.T. Ting reports grants from NIH/NCI and other support from Rome Therapeutics during the conduct of the study; other support from PanTher Therapeutics, TellBio, Inc., ImproveBio, Inc., Tekla Capital, Sonata Therapeutics, Moderna, Ikena Oncology, Pfizer, Foundation Medicine, Inc., NanoString Technologies, grants from ACD-Biotechne, Ava Lifescience GmbH, and Incyte Pharmaceuticals outside the submitted work; in addition, D.T. Ting has a patent for US20220098678A1 pending and licensed to Rome Therapeutics, a patent for US20200017856A1 pending and licensed to Rome Therapeutics, and a patent for US20220110963A1 pending and licensed to Rome Therapeutics. M.P. Rout reports a patent for 63/423,696 pending. J. LaCava reports grants, personal fees, and other support from Rome Therapeutics, Oncolinea, personal fees from Transposon Therapeutics, grants from Refeyn, and Ribon Therapeutics outside the submitted work; in addition, J. LaCava has a patent for Ultrasensitive Assays for Detection of ORF1p in Biofluids pending. D.R. Walt reports personal fees and other support from Quanterix Corporation outside the submitted work; in addition, D.R. Walt has a patent for application pending. K.H. Burns reports grants from NIH/NCI, Break Through Cancer, Earlier.Org, Minnesota Ovarian Cancer Alliance, Dana-Farber Cancer Institute, Friends of Dana-Farber Cancer Institute, and Dana-Farber/Harvard Cancer Center during the conduct of the study; personal fees and other support from Rome Therapeutics, Oncolinea/PrimeFour Therapeutics, Transposon Therapeutics, and Scaffold Therapeutics outside the submitted work; in addition, K.H. Burns has a patent for Ultrasensitive Assays for Detection of ORF1p in Biofluids issued. No disclosures were reported by the other authors.

Authors' Contributions

M.S. Taylor: Conceptualization, resources, data curation, formal analysis, supervision, funding acquisition, validation, investigation, visualization, methodology, writing–original draft, project administration, writing–review and editing. **C. Wu:** Conceptualization, resources, data curation, formal analysis, supervision, funding acquisition, validation, investigation, visualization, methodology, writing–original draft, project administration, writing–review and editing. **P.C. Fridy:** Conceptualization, resources, data curation, formal analysis, validation, investigation, visualization, writing–review and editing. **S.J. Zhang:** Formal analysis, validation, investigation, writing–review and editing. **Y. Senussi:** Data curation, formal analysis, validation, investigation, methodology, writing–review and editing. **J.C. Wolters:** Conceptualization, data curation, formal analysis, validation, investigation, methodology, writing–review and editing. **T. Cajuso:** Data curation, formal analysis, validation, investigation, visualization, writing–review and editing. **W. Cheng:** Formal analysis, investigation, project administration, writing–review and editing. **J.D. Heaps:** Investigation, writing–review and editing. **B.D. Miller:** Investigation, writing–review and editing. **K. Mori:** Data curation, formal analysis, investigation, visualization, methodology, writing–review and editing. **L. Cohen:** Conceptualization, investigation, writing–review and editing. **H. Jiang:** Investigation, writing–review and editing. **K.R. Molloy:** Investigation, methodology, writing–review and editing. **B.T. Chait:** Resources, supervision, methodology, project administration, writing–review and editing. **M.G. Goggins:** Resources, investigation, writing–review and editing. **I. Bhan:** Resources, investigation, writing–review and editing. **J.W. Franses:** Resources, investigation, writing–review and editing. **X. Yang:** Resources, investigation, writing–review and editing. **M. Taplin:** Resources, investigation, writing–review and editing. **X. Wang:** Resources, investigation, writing–review and editing. **D.C. Christiani:** Resources, investigation, writing–review and editing. **B.E. Johnson:** Resources, investigation, writing–review and editing. **M. Meyerson:** Resources, investigation, writing–review and editing. **R. Uppaluri:** Resources, investigation, writing–review and editing. **A. Egloff:** Resources, investigation, writing–review and editing. **E.N. Denault:** Resources, investigation, writing–review and editing. **L.M. Spring:** Resources, investigation, writing–review and editing. **T.-L. Wang:** Resources, investigation, writing–review and editing. **I.-M. Shih:** Resources, investigation, writing–review and editing. **J.E. Fairman:** Visualization, writing–review and editing. **E. Jung:** Resources, investigation, writing–review and editing. **K. Arora:** Investigation, writing–review and editing. **O.H. Yilmaz:** Investigation, writing–review and editing. **S. Cohen:** Resources, supervision, investigation, writing–review and editing. **T. Sharova:** Resources, investigation, writing–review and editing. **G. Chi:** Resources, investigation, writing–review and editing. **B.L. Norden:** Resources, data curation, validation, investigation, writing–review and editing. **Y. Song:** Resources, investigation, writing–review and editing. **L.T. Nieman:** Resources, data curation, supervision, investigation, writing–review and editing. **L. Pappas:** Resources, data curation, formal analysis, investigation, writing–review and editing. **A.R. Parikh:** Conceptualization, resources, supervision, investigation, writing–review and editing. **M.R. Strickland:** Conceptualization, resources, data curation, formal analysis, investigation, visualization, methodology,

writing–review and editing. **R.B. Corcoran:** Resources, supervision, investigation, writing–review and editing. **T. Mustelin:** Resources, investigation, writing–review and editing. **G. Eng:** Resources, formal analysis, investigation, visualization, writing–review and editing. **O.H. Yilmaz:** Conceptualization, resources, supervision, investigation, methodology, writing–review and editing. **A.T. Chan:** Conceptualization, resources, data curation, formal analysis, supervision, funding acquisition, validation, investigation, visualization, methodology, writing–original draft, project administration, writing–review and editing. **U.A. Matulonis:** Resources, investigation, writing–review and editing. **S.J. Skates:** Conceptualization, data curation, formal analysis, supervision, funding acquisition, validation, investigation, methodology, writing–review and editing. **B.R. Rueda:** Resources, supervision, funding acquisition, validation, investigation, visualization, writing–review and editing. **R. Drapkin:** Conceptualization, resources, investigation, methodology, writing–review and editing. **S.J. Klempner:** Conceptualization, resources, data curation, formal analysis, supervision, funding acquisition, validation, investigation, visualization, methodology, project administration, writing–review and editing. **V. Deshpande:** Conceptualization, resources, supervision, funding acquisition, validation, investigation, visualization, methodology, project administration, writing–review and editing. **D.T. Ting:** Conceptualization, resources, supervision, funding acquisition, validation, visualization, project administration, writing–review and editing. **M.P. Rout:** Conceptualization, resources, supervision, funding acquisition, investigation, writing–review and editing. **J. LaCava:** Conceptualization, resources, data curation, formal analysis, supervision, funding acquisition, validation, investigation, visualization, methodology, project administration, writing–review and editing. **D.R. Walt:** Conceptualization, resources, supervision, funding acquisition, investigation, methodology, writing–original draft, project administration, writing–review and editing. **K.H. Burns:** Conceptualization, resources, supervision, funding acquisition, investigation, methodology, writing–original draft, project administration, writing–review and editing.

Acknowledgments

We mourn the loss of our dear colleague, Lawrence R. Zukerberg, who died unexpectedly during the preparation of this manuscript and made key contributions to our studies of ORF1p in tissue. We thank Bert Vogelstein for plasma samples from colorectal cancer patients. We are grateful to Phil Cole for resources for protein expression and purification and helpful discussions and to Andrew Kruse and Edward Harvey for helpful discussions regarding nanobodies. We thank Zuzana Tothova for the helpful discussion and review of the manuscript. This work was supported by NIH grants R01GM130680 (K.H. Burns), K08DK129824 (M.S. Taylor), F32EB029777 (C. Wu), R01CA240924 (D.T. Ting), U01CA228963 (D.T. Ting), P41 GM109824 (M.P. Rout and B.T. Chait), T32CA009216 (M.S. Taylor and G. Eng), U01CA233364, U2CCA271871, U01CA152990 (S.J. Skates), R01GM126170 (J. LaCava), P50CA228991 Ovarian SPORE (E. Jung, T.-L. Wang, I.-M. Shih, and R. Drapkin), P50CA240243 Ovarian SPORE (U.A. Matulonis), P30CA006516 Incubator (M.S. Taylor, D.T. Ting, B.R. Rueda, S.J. Skates, S.J. Klempner, and K.H. Burns), Dana-Farber/Harvard Cancer Center (DF/HCC) SPORE in Gastrointestinal Cancer, NIH/NCI P50CA127003; Break *Through* Cancer (K.H. Burns); Earlier.Org (K.H. Burns and D.R. Walt); Minnesota Ovarian Cancer Alliance (K.H. Burns); DOD W81XWH-22-1-0852 (E. Jung and R. Drapkin); Canary Foundation (R. Drapkin); Gray Foundation (E. Jung and R. Drapkin); The Concord (MA) Detect Ovarian Cancer Early Fund (S.J. Skates), Good Ventures (Open Philanthropy Project); Friends of Dana-Farber Cancer Institute; Dana-Farber Cancer Institute; and the DF/HCC; ACD-Biotechne (D.T. Ting and V. Deshpande); Robert L. Fine Cancer Research Foundation (D.T. Ting); Worldwide Cancer Research grant 19-0223 (J. LaCava); Robertson Therapeutic Development Fund (J. LaCava); Nile Albright Research Foundation (B.R. Rueda); Vincent Memorial Research Foundation (B.R. Rueda); Stand Up To Cancer Gastric Cancer Interception Research Team Grant (SU2C-AACR-DT-30-20, A.T. Chan, S.J. Skates and D.T. Ting, administered by the American Association for Cancer Research, the Scientific Partner of SU2C).

The publication costs of this article were defrayed in part by the payment of publication fees. Therefore, and solely to indicate this fact, this article is hereby marked "advertisement" in accordance with 18 USC section 1734.

Note

Supplementary data for this article are available at Cancer Discovery Online (http://cancerdiscovery.aacrjournals.org/).

Received March 24, 2023; revised August 9, 2023; accepted September 8, 2023; published first September 12, 2023.

REFERENCES

1. Siegel RL, Miller KD, Fuchs HE, Jemal A. Cancer statistics, 2022. CA Cancer J Clin 2022;72:7–33.
2. Sawyers CL. The cancer biomarker problem. Nature 2008;452:548–52.
3. Crosby D, Bhatia S, Brindle KM, Coussens LM, Dive C, Emberton M, et al. Early detection of cancer. Science 2022;375:eaay9040.
4. Ignjatovic V, Geyer PE, Palaniappan KK, Chaaban JE, Omenn GS, Baker MS, et al. Mass spectrometry-based plasma proteomics: considerations from sample collection to achieving translational data. J Proteome Res 2019;18:4085–97.
5. Jamshidi A, Liu MC, Klein EA, Venn O, Hubbell E, Beausang JF, et al. Evaluation of cell-free DNA approaches for multi-cancer early detection. Cancer Cell 2022;40:1537–49.
6. Bast RC Jr, Lu Z, Han CY, Lu KH, Anderson KS, Drescher CW, et al. Biomarkers and strategies for early detection of ovarian cancer. Cancer Epidemiol Biomarkers Prev 2020;29:2504–12.
7. Menon U, Gentry-Maharaj A, Burnell M, Singh N, Ryan A, Karpinskyj C, et al. Ovarian cancer population screening and mortality after long-term follow-up in the UK Collaborative Trial of Ovarian Cancer Screening (UKCTOCS): a randomised controlled trial. Lancet 2021;397:2182–93.
8. Rodić N, Sharma R, Sharma R, Zampella J, Dai L, Taylor MS, et al. Long interspersed element-1 protein expression is a hallmark of many human cancers. Am J Pathol 2014;184:1280–6.
9. Ardeljan D, Wang X, Oghbaie M, Taylor MS, Husband D, Deshpande V, et al. LINE-1 ORF2p expression is nearly imperceptible in human cancers. Mob DNA 2020;11:1.
10. Lee E, Iskow R, Yang L, Gokcumen O, Haseley P, Luquette LJ 3rd, et al. Landscape of somatic retrotransposition in human cancers. Science 2012;337:967–71.
11. Helman E, Lawrence MS, Stewart C, Sougnez C, Getz G, Meyerson M. Somatic retrotransposition in human cancer revealed by whole-genome and exome sequencing. Genome Res 2014;24:1053–63.
12. Rodriguez-Martin B, Alvarez EG, Baez-Ortega A, Zamora J, Supek F, Demeulemeester J, et al. Pan-cancer analysis of whole genomes identifies driver rearrangements promoted by LINE-1 retrotransposition. Nat Genet 2020;52:306–19.
13. Burns KH. Transposable elements in cancer. Nat Rev Cancer 2017;17:415–24.
14. McKerrow W, Kagermazova L, Doudican N, Frazzette N, Kaparos EI, Evans SA, et al. LINE-1 retrotransposon expression in cancerous, epithelial and neuronal cells revealed by 5′ single-cell RNA-Seq. Nucleic Acids Res 2023;51:2033–45.
15. Pisanic TR 2nd, Asaka S, Lin SF, Yen TT, Sun H, Bahadirli-Talbott A, et al. Long interspersed nuclear element 1 retrotransposons become deregulated during the development of ovarian cancer precursor lesions. Am J Pathol 2019;189:513–20.
16. Cohen L, Cui N, Cai Y, Garden PM, Li X, Weitz DA, et al. Single molecule protein detection with attomolar sensitivity using droplet digital enzyme-linked immunosorbent assay. ACS Nano 2020;14:9491–501.

17. Rajurkar M, Parikh AR, Solovyov A, You E, Kulkarni AS, Chu C, et al. Reverse transcriptase inhibition disrupts repeat element life cycle in colorectal cancer. Cancer Discov 2022;12:1462–81.
18. Solyom S, Ewing AD, Rahrmann EP, Doucet T, Nelson HH, Burns MB, et al. Extensive somatic L1 retrotransposition in colorectal tumors. Genome Res 2012;22:2328–38.
19. Ewing AD, Gacita A, Wood LD, Ma F, Xing D, Kim MS, et al. Widespread somatic L1 retrotransposition occurs early during gastrointestinal cancer evolution. Genome Res 2015;25:1536–45.
20. Scott EC, Gardner EJ, Masood A, Chuang NT, Vertino PM, Devine SE. A hot L1 retrotransposon evades somatic repression and initiates human colorectal cancer. Genome Res 2016;26:745–55.
21. Cajuso T, Sulo P, Tanskanen T, Katainen R, Taira A, Hanninen UA, et al. Retrotransposon insertions can initiate colorectal cancer and are associated with poor survival. Nat Commun 2019;10:4022.
22. Doucet-O'Hare TT, Rodic N, Sharma R, Darbari I, Abril G, Choi JA, et al. LINE-1 expression and retrotransposition in Barrett's esophagus and esophageal carcinoma. Proc Natl Acad Sci U S A 2015;112:E4894–900.
23. Katz-Summercorn AC, Jammula S, Frangou A, Peneva I, O'Donovan M, Tripathi M, et al. Multi-omic cross-sectional cohort study of pre-malignant Barrett's esophagus reveals early structural variation and retrotransposon activity. Nat Commun 2022;13:1407.
24. Xia Z, Cochrane DR, Tessier-Cloutier B, Leung S, Karnezis AN, Cheng AS, et al. Expression of L1 retrotransposon open reading frame protein 1 in gynecologic cancers. Hum Pathol 2019;92:39–47.
25. Carter V, LaCava J, Taylor MS, Liang SY, Mustelin C, Ukadike KC, et al. High prevalence and disease correlation of autoantibodies against p40 encoded by long interspersed nuclear elements in systemic lupus erythematosus. Arthritis Rheumatol 2020;72:89–99.
26. Wu C, Dougan TJ, Walt DR. High-throughput, high-multiplex digital protein detection with attomolar sensitivity. ACS Nano 2022;16:1025–35.
27. Jacobs IJ, Menon U, Ryan A, Gentry-Maharaj A, Burnell M, Kalsi JK, et al. Ovarian cancer screening and mortality in the UK Collaborative Trial of Ovarian Cancer Screening (UKCTOCS): a randomised controlled trial. Lancet 2016;387:945–56.
28. Wylie A, Jones AE, D'Brot A, Lu WJ, Kurtz P, Moran JV, et al. p53 genes function to restrain mobile elements. Genes Dev 2016;30:64–77.
29. De Cecco M, Ito T, Petrashen AP, Elias AE, Skvir NJ, Criscione SW, et al. L1 drives IFN in senescent cells and promotes age-associated inflammation. Nature 2019;566:73–8.
30. Simon M, Van Meter M, Ablaeva J, Ke Z, Gonzalez RS, Taguchi T, et al. LINE1 derepression in aged wild-type and SIRT6-deficient mice drives inflammation. Cell Metab 2019;29:871–85.
31. Fridy PC, Li Y, Keegan S, Thompson MK, Nudelman I, Scheid JF, et al. A robust pipeline for rapid production of versatile nanobody repertoires. Nat Methods 2014;11:1253–60.
32. Mast FD, Fridy PC, Ketaren NE, Wang J, Jacobs EY, Olivier JP, et al. Highly synergistic combinations of nanobodies that target SARS-CoV-2 and are resistant to escape. Elife 2021;10:e73027.
33. Wolters JC, Ciapaite J, van Eunen K, Niezen-Koning KE, Matton A, Porte RJ, et al. Translational targeted proteomics profiling of mitochondrial energy metabolic pathways in mouse and human samples. J Proteome Res 2016;15:3204–13.
34. Kaplan EL, Meier P. Nonparametric estimation from incomplete observations. J Am Statist Assoc 1958;53:457–81.
35. Cox DR. Regression models and life-tables. J R Stat Soc Series B Stat Methodol 1972;34:187–202.